SCIENCE CHINA
Physics, Mechanics & Astronomy

• Article •

May 2014 Vol.57 No.5: 994–1000
doi: 10.1007/s11433-014-5407-3

Compositional evolution of lava plains in the Syria-Thaumasia Block, Mars†

HUANG Jun[1,2*] & XIAO Long[1*]

[1] *Planetary Science Institute, China University of Geosciences, Wuhan 430074, China;*
[2] *Mars Space Flight Facility, Arizona State University, Tempe, AZ, USA*

Received December 12, 2013; accepted January 17, 2014; published online March 13, 2014

Tharsis is the most prominent volcanic province on Mars, yet the compositions of lava flows and how composition relates to the development of Tharsis are poorly known. Most of Tharsis is covered with air-fall dust, which inhibits spectroscopic determination of lava mineralogy. The Syria-Thaumasia Block (STB) is a complex tectono-volcanic province closely related to the Tharsis bulge. The lava plains of STB have different emplacement ages, which provide an opportunity to examine whether magma composition changed with the evolution of Tharsis. In this study, we assessed the lava plains using Thermal Emission Spectrometer (TES) data. Using derived physical properties, we targeted dust-free regions from four different-aged geological units' surfaces and determined the mineralogical composition by modeling the average TES surface spectrum from each of the four surfaces. All units have similar mineralogy but the younger two units have elevated abundance of high-SiO_2 phases. The spatial distribution of wrinkle ridges indicates lava plains of unit HNr (older ridged plains material) and Hr (younger ridged plains material) were emplaced before the rise of Tharsis, whereas Hsl (flows of lower member) and Hsu (upper member) were emplaced after Tharsis uplift was initiated. We show that the magma composition differed in the lava plains of STB after the uplift of Tharsis. This study further characterizes early martian magma composition and evolution.

Syria-Thaumasia Block, lava plains, volcanism, Tharsis, Mars

PACS number(s): 96.30.Gc, 91.45.Jg, 07.07.Df

Citation: Huang J, Xiao L. Compositional evolution of lava plains in the Syria-Thaumasia Block, Mars. Sci China-Phys Mech Astron, 2014, 57: 994–1000, doi: 10.1007/s11433-014-5407-3

1 Introduction

The volcanic history of Mars is long [1,2] and complex [3], and Tharsis is the most prominent tectono-volcanic province. The morphology of volcanic features on Tharsis has been extensively described [4]. Physical characteristics (density, viscosity and eruption rate) of lavas that formed in Tharsis have been calculated through inversion of gravity and topographic data [5] and terrestrial fluid dynamic modeling [6,7]. It is necessary to complement morphological and physical observations with compositional data, which will better constrain volcanic diversity in the Tharsis region, and enable comparison of Tharsis volcanics to global volcanics on Mars.

Global Hesperian volcanics were determined with Gamma Ray Spectrometer (GRS) data to be more SiO_2-rich than later Amazonian volcanics [8], and this global trend may apply to Tharsis volcanics. The silicate mineralogical composition of Tharsis volcanics was determined for portions of Tharsis in previous studies [9–12]. These studies, however, concentrated on determining global spectral and mineralogical differences on Mars. Global composition studies are too broad to have examined mineralogical diversity within Tharsis and understand it in terms of the regional geology.

*Corresponding author (HUANG Jun, email: junhuang@cug.edu.cn; XIAO Long, email: longxiao@cug.edu.cn)
†Contributed by XIAO Long (Associate Editor)

In addition, the Tharsis region is largely dust covered and significant portions of the volcanic surface are obscured from spectral observation [13]. Spectroscopically assessing volcanic compositions in Tharsis requires non-dusty surfaces [14], but understanding the diversity requires a focused investigation that is centered on regional geology in addition to seeking "dust-free" regions.

In this study, we focus on the Syria-Thaumasia Block (STB), which is a complex tectono-volcanic province comprising a southern portion of the Tharsis bulge. Most of STB is comprised of lava plains of different ages, ranging from Late Noachian to Late Hesperian [15]. We examine how erupted magma compositions varied over time in STB by using Thermal Emission Spectrometer (TES) data to determine the mineralogical composition of different-aged lava plains.

2 Geologic setting and history

The STB lies at the southern edge of the Tharsis bulge (Figure 1(a)). It consists of lava plains (Syria, Solis, Sinia and Thaumasia) and is bounded by an arcuate region of higher topography (Claritas Fossae, Thaumasia Highlands and Coprates Rise). STB is bounded by Valles Marineris to the north. The Thaumasia Highlands, which extend approximately 3000 km in length and rise approximately 4 km above the adjacent terrains, are fractured by extensive systems of rifts and graben harboring massifs and ancient volcanoes [2,15]. The lava plains (Syria, Solis, Sinai, and Thaumasia) have a cumulative area of ~3×10^6 km^2 and they are characterized by a southeastward regional slope (Figure 1(a)). The Syria Planum, located in northwestern STB, is the highest elevation lava plain and it is considered to be a volcanotectonic center that was active from Noachian to early Amazonian period [15–17]. A swarm of tens of coalesced shallow volcanic edifices were identified on southern Syria Planum that are typically 10–30 km in diameter, 0.1–0.2 km high, and have slopes around 0.5° [18]. Southern Sinai Planum and Thaumasia Planum are characterized by extensive wrinkle ridges, which are thought to result from compressional folding and faulting of surface units [19–21]. The northern Sinai Planum is covered heavily by dust.

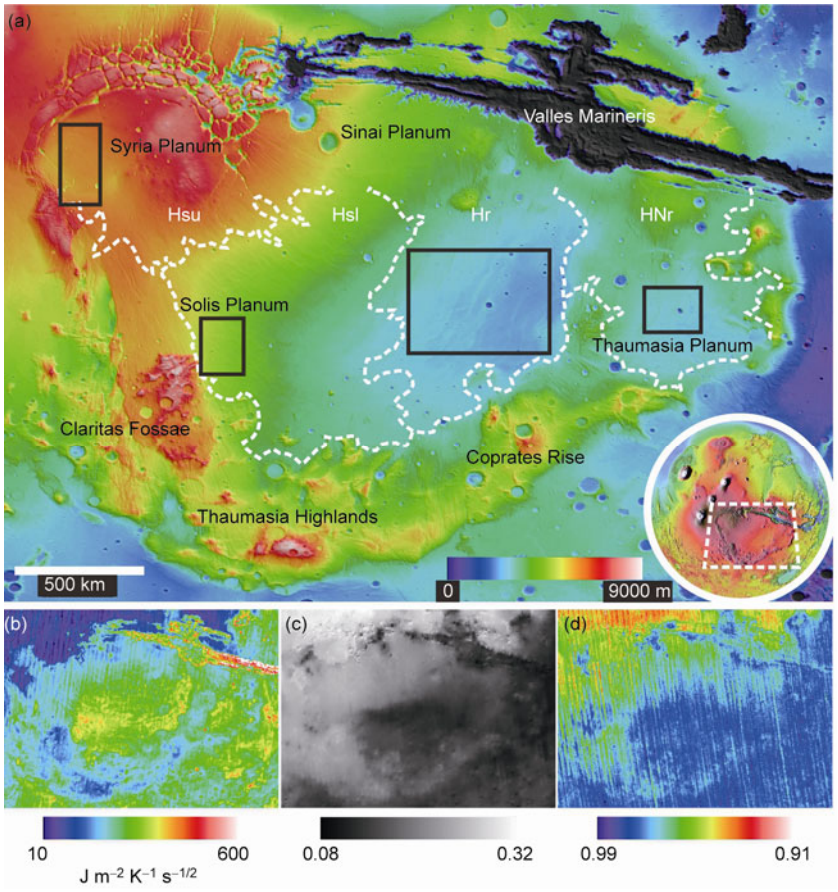

Figure 1 Overview of STB, (a)–(d) with the same latitude and longitude ranges (247–305.5°E, 2–44°S). (a) MOLA color coded map [47] overlain on MOLA shaded relief map. Black boxes show the coordinate constraints of TES spectra for each unit (HNr: 292.5–296.5°E, 21.5–26°S; Hr: 275.5–285.5°E, 19–26.5°S; Hsl: 261–264°E, 24–28°S; Hsu: 251–254°E, 10.5–16°S). White dash lines are boundaries [22] of unit HNr (older ridged plains material), Hr (younger ridged plains material), Hsl (flows of lower member) and Hsu (upper member). (b) TES nightside median thermal inertia map [23]. (c) TES albedo map [24]. (d) DCI map [13].

Dohm and Tanaka [15] mapped several geological units within STB, and derived relative age relationships for the lava plains (Figure 1(a)) based on superposition and crater counts. They divided the lava plains into four chronostratigraphic units [22]. From oldest to youngest, the units are HNr (older ridged plains material), Hr (younger ridged plains material), Hsl (flows of lower member) and Hsu (upper member). HNr encompasses Thaumasia Planum. Hr includes Sinai Planum and eastern Solis Planum. Hsl marks the flows of western Solis, and Hsu covers Syria Planum. Using these unit ages and their distribution, we determined how lava composition varied with time in the STB by determining the average mineralogical composition of each unit.

3 Methods

In this study, we primarily used the JMARS (http://jmars.asu.edu/) and Davinci (http://davinci.asu.edu) software packages developed by Mars Space Flight Facility at Arizona State University to query, process, visualize, and interrelate different datasets in the study region. Maps (provided by JMARS) of TES nightside median thermal inertia (Figure 1(b)) [23], TES albedo (Figure 1(c)) [24], and TES Dust Cover Index (DCI) (Figure 1(d)) [13] were used to qualitatively inspect the surface physical properties and select a sub-region within each of the four geologic map units to use for spectral analysis.

Thermal inertia represents a material's resistance to temperature changes, and it can be related to an effective particle size, assuming unconsolidated surfaces with a uniform grain size [25,26], while albedo and DCI indicate whether the surface is covered by air-fall dust. For each map unit, we defined one study region (a sub-region) based on contiguous relatively high thermal inertia (> ~230 J m^{-2} K^{-1} $s^{-1/2}$ for unit Hsl, Hr and HNr and > ~110 J m^{-2} K^{-1} $s^{-1/2}$ for unit Hsu). The thermal inertia (from TES Data Archive: tes.asu.edu/data_tool/) is associated with each TES emissivity spectral observation and derived from the method described elsewhere [27]. Materials with these thermal inertia values (Table 1) are suitable for quantitative thermal infrared spectral analysis [28]; because they indicate that a significant portion of the surface is made of particles large enough to sufficiently minimize the effects of multiple scattering. These materials provide a good opportunity to look into the compositions of surface materials (volcanic origin) of its unit. Previous studies have shown that two-layer model for thermal inertia is critical for detail thermophysical analysis [23]. However, the main scope of this study was to analyze the compositions of different lava plains in STB, therefore we did not carry out more detailed thermophysical analysis.

For each sub-region, TES emissivity spectra were extracted using query constraints similar to Rogers et al. [29]: target temperature > 270 K, emission angle < 30, orbit range 1683–7000, total ice extinction < 0.04 and total dust extinction < 0.15. We included DCI > 0.97 as an additional constraint to further avoid TES data significantly affected by surface dust [13]. We grouped and averaged the TES emissivity spectra by orbit and removed the atmospheric components (Table 2) using the linear spectral unmixing (deconvolution) method [30,31].

We averaged the atmospherically corrected spectra (Table 1) from each sub-region to produce an average surface emissivity spectrum for each sub-region. We derived the modal mineralogy for each study region using a spectral deconvolution method [32,33] to model the average spectrum with a mixture of library minerals (Table 2) over the spectral range of 1301–230 cm^{-1} (825–507 cm^{-1} was excluded due to strong feature of CO_2 in the atmosphere). For simplicity, we assume the average spectrum and mineral composition derived for each sub-region represents the surface compositions of the entire corresponding map unit: HNr, Hr, Hsl and Hsu. Since we have averaged a bunch of TES spectra for each unit (Table 1), local-scale enrichments in a single mineral group may be obscured, and any deviation from the modeled composition would not be captured.

4 Results

Within the STB region, thermal inertia becomes lower with increasing elevation, as can be observed in Figures 1(a), 1(b) and Table 1. Thermal inertia and albedo vary laterally within each geologic unit (Table 1), and the surface materials within each sub-region are relatively dust-free and suitable for spectral analysis based on experience of previous compositional studies [11,28].

Averaged surface emissivity spectra from four sub-

Table 1 Summary of thermophysical properties and the number of TES spectra for each sub-region

Geological unit	Symbol	Surface model age	Thermal inertia (J m^{-2} K^{-1} $s^{-1/2}$)	TES Albedo	# of TES spectra averaged	DCI
Syria Planum	Hsu	Middle Hesperian to Late Hesperian	111–251	0.12–0.24	1092	0.97–0.99
Solis Planum	Hsl	Middle Hesperian	231–664	0.15–0.23	1624	0.97–0.99
Southern Sinai Planum	Hr	Early Hesperian to Middle Hesperian	247–702	0.08–0.18	4663	0.97–0.99
Thaumasia Planum	HNr	Late Noachian to Early Hesperian	280–486	0.11–0.17	3227	0.97–0.99

Table 2 Spectral library[a)]

Spectral group	End-Member
Quartz	Quartz BUR-4120
Feldspar	Microcline BUR-3460
	Albite WAR-0244
	Oligoclase WAR-5804
	Andesine BUR-240
	Labradorite WAR-4525
	Bytownite WAR-1384
	Anorthite BUR-340
	Orthoclase WAR-RGSAN01
	Shocked An 22.6 GPa
	Shocked An 56.3 GPa
Low Calcium Pyroxene	Bronzite NMNH-93527
	Enstatite HS-9.4B
	Bronzite BUR-1920
	Avg. Lindsley pigeonite
High Calcium Pyroxene	Diopside WAR-6474
	Augite NMNH-9780
	Augite NMHN-122302
	Hedenbergite manganoan DSM-HED01
Olivine	Forsterite BUR-3720A
	Fayalite WAR-RGFAY01
	KI 3362 Fo60
	KI 3115 Fo68
	KI 3373 Fo35
	KI 3008 Fo10
High-silica	K-rich Glass
	SiO_2 Glass
	opal-A (01-011)
	Al-Opal
	Crystalline heulandite
	Crystalline stilbite
Iron Oxide	Average Martian Hematite
Carbonate	Calcite C40
	Dolomite C20
Sulfate	Anhydrite ML-S9
	Gypsum ML-S6
Mica	Biotite BUR-840
	Muscovite WAR-5474
Serpentine	Serpentine HS-8.4B
	Antigorite NMNH-47108
Sheet-silicate	Illite granular IMt-2 minus 60% bb[b)]
	Ca-montmorillonite solid STx-1
	saponite <0.2 mic plus 60% bb[b)]
Amphibole	Magnesiohastingsite HS-115.4B
	Actinolite HS-116.4B
	Magnesiohornblende WAR-0354
Atmosphere	CO_2
	Dust, low CO_2
	Dust, high CO_2
	Water vapor
	Water ice cloud (high latitude)
	Water ice cloud (low latitude)

a) Spectra are from the ASU spectral library (http://speclib.asu.edu/) [46].

b) Blackbody was subtracted from the spectrum to produce comparable spectral contrast to that of other solid clays in the ASU library.

regions are shown in Figure 2. The differences between each spectral shape are subtle, but several points can be noted. Firstly, the spectral shape of unit Hsl is more similar to Surface Type 2 [30] in shorter wavelength, while other spectral shapes are more like Surface Type 1. Secondly all the spectral shapes are similar at longer wavelengths and more similar to Surface Type 1 (beyond 30 μm), but the spectral shapes of unit Hsl and Hsu are slightly different in ~22–26 μm from the other spectra. Thirdly, the spectral shape of Hsu is a slightly convex upward near ~10–12 μm, which may indicate the presence of some finer-grained surface materials, and potentially could explain the lower thermal inertia and higher albedo of this unit relative to the other three units (Table 1). A similar spectral characteristic was observed in southern Acidalia, which was potentially due to a thin dust cover in that region [29].

Feldspar, high-Ca pyroxene (HCP), low-Ca pyroxene (LCP) and high-silica phases were the principal mineral groups modeled for all lava plains (Figure 3 and Table 3). Olivine, sulfate and carbonate were modeled around the detection limit [34]. Generally, the younger units (Hsl and Hsu) had a higher concentration of high-silica phases than the older units. High-silica glass was the main high-silica phases modeled in the spectral fit. The other mineral groups were modeled in similar amounts for all the units. The results are consistent with an overall basaltic composition for the STB lava plains, and are consistent with previous global infrared spectroscopic studies [9–12].

5 Discussion

Extensive lava emplacement in the plains of STB has been observed in previous studies [15,18], but the mechanism was not well known. Direct observations of dikes in Thaumasia Planum [35] and indirect implication of dike intrusion complexes from Tharsis-radial graben systems [36] may have been a main mechanism for building lava plains for unit HNr and regions with extensive graben (unit Hsu and western Hsl). The extensive wrinkle ridges in unit HNr and Hr were formed due to regional compression [19–21]. A thin-shell flexural model of Tharsis loading indicated widely distributed compression throughout the lava plains in STB [37], and the observed extension directions of wrinkle ridges in unit HNr and Hr are consistent with the compression stress field of that model. This implies the lava plains of these two units formed before and the wrinkle ridges formed after the rise of Tharsis. Conversely, there is no wrinkle ridges observed in units Hsl and Hsu, although compressional stress existed after emplacement of both units [37]. This implies these two units formed after the rise of Tharsis. Although the surface materials can be transported by aeolian and impact processes, we interpret that they are locally derived and their TES spectra represent local compositions based on the following reasons. Firstly, parti-

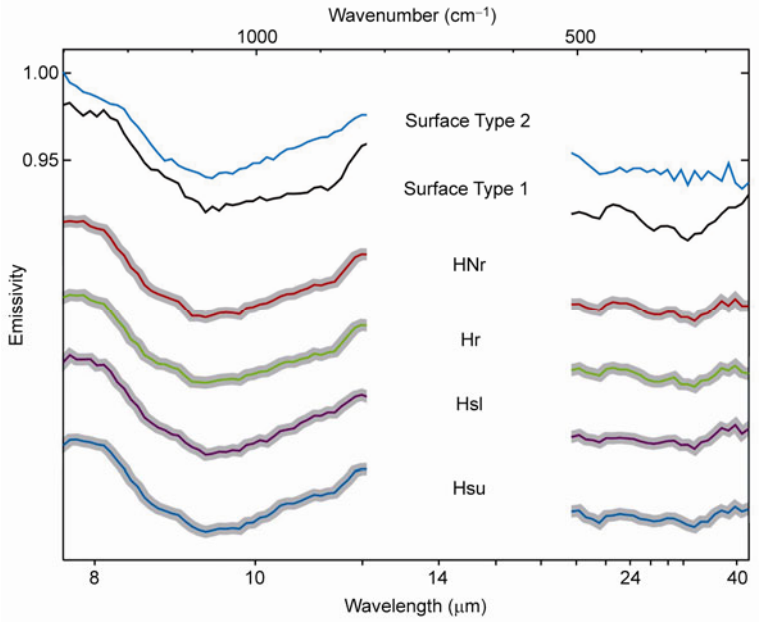

Figure 2 Averaged surface emissivity spectra from geological units HNr, Hr, Hsl and Hsu, for which modal mineralogy is derived. Shadows indicate the standard deviation of all the spectra averaged. Spectra are offset for clarity and shown compared to the global Surface Type 1 and Type 2 spectra [30].

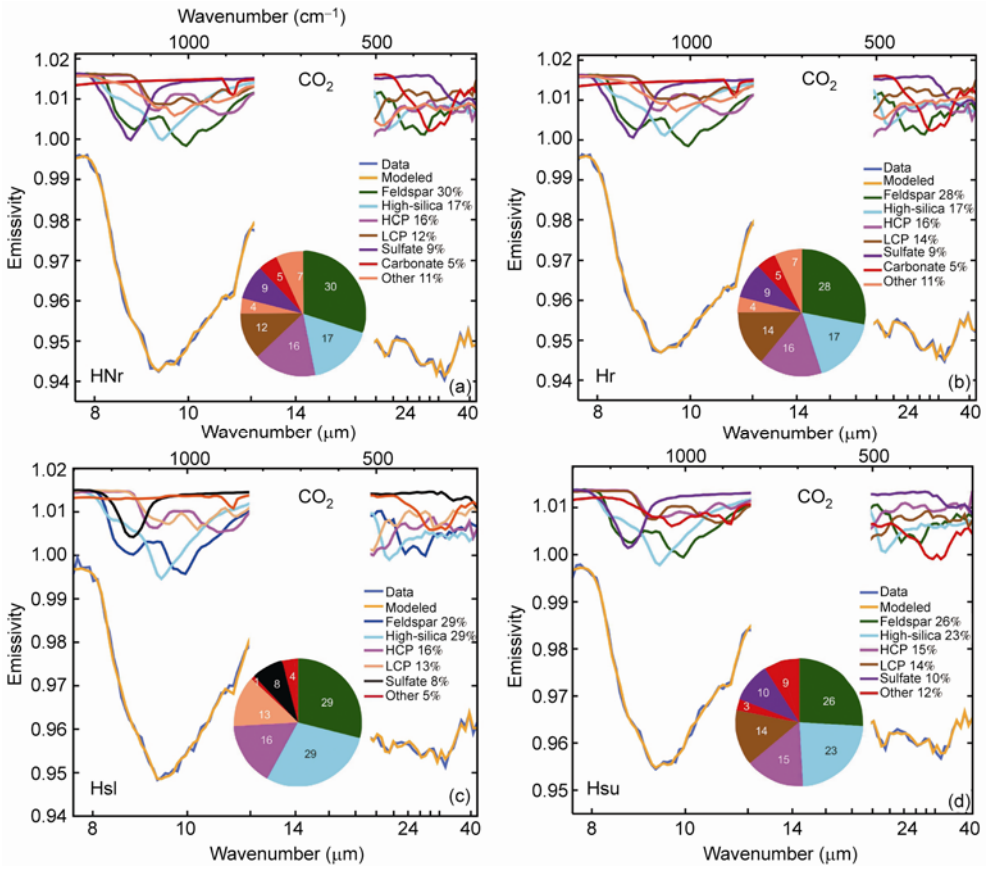

Figure 3 Modeled mineral abundances of surface materials of lava plains in STB (RMS errors are presented in Table 3). Averaged atmospheric corrected TES spectra for unit HNr, Hr, Hsl and Hsu are shown with their corresponding best-fit modeled spectrum from linear deconvolution. The spectra of end-member minerals used in the fit are also shown.

Table 3 Derived modal mineralogy[a)]

	HNr		Hr		Hsl		Hsu	
Feldspar	30	(5)	28	(5)	29	(3)	26	(3)
High-silica	17	(4)	17	(3)	29	(4)	23	(3)
HCP	16	(4)	16	(4)	16	(3)	15	(4)
LCP	12	(5)	14	(5)	13	(2)	14	(3)
Olivine	4	(2)	4	(2)	1	(2)	3	(2)
Sulfate	9	(2)	9	(1)	8	(1)	10	(1)
Carbonate	5	(1)	5	(1)	3	(0)	4	(0)
Other	7		7		1		5	
RMS (%)	0.08		0.09		0.11		0.07	

a) Values are percent, rounded to the nearest whole number. Number with parentheses indicate root-mean-square (RMS) errors for derived abundance of each mineral group.

cles would be entrained by wind infrequently because of the low atmospheric pressure experienced at the high elevations of the STB [38]. Secondly, particles are unlikely to survive saltation transport over longer distances on Mars [11], especially if high wind speeds are required to move particles [39]. Thirdly, impact mixing of materials in the STB should have been relatively low because the lava plains were emplaced well after Late Heavy Bombardment. Lastly, during an impact the majority of materials remain relatively local [40]. Previous regional spectroscopy studies applied this assumption of locally derived materials with similar thermophysical properties [11,28].

The spectral deconvolution results show composition variations: younger units have higher abundances of high-silica phases than the old units. The unit Hsu is possibly covered with thin dust as inferred from the spectral shape (Figure 2), and model results for Hsu may be less accurate. It is possible that the high-silica phases of unit Hsu were under modeled which indicates Hsu could be similar to Hsl in composition. The TES-derived composition results are consistent with SiO_2 concentration trend derived from GRS data [41] over the Tharsis region [8] and density variations (indication of composition variations) among lavas of Tharsis volcanic features derived from gravity data [5]. There might be a coincidence between the variations in composition results and the differences in geomorphologic characteristics of lava features throughout all the units: possible cinder cones and small shields in unit Hsu [42]; coalesced shallow volcanic edifices in unit Hsl [18]; long distance lava flows with imbedded lava channels and tubes [43], but no volcanic edifices in unit Hr and HNr.

Thus, the compositional results (different amounts of high-silica phases), the spatial distribution of wrinkle ridges (lava emplacement happened before wrinkle ridges in unit HNr and Hr, but after wrinkle ridges in unit Hsl and Hsu), and relative surface age [22] indicate lava composition changed subsequent to the rise of Tharsis.

The reason for compositional variations is complex and we suggest two possible explanations which cannot be distinguished based on the results. If the magma of all the lava plains in STB was from the same source, the silicic content in the magma would increase as it evolved. More mafic lava would have been removed from the source to form units HNr and Hr [35] during earlier melting events. The only material remaining was less mafic and therefore the younger lava was more silicic to form units Hsl and Hsu. Another contributing factor is magma density. As the Tharsis bulge grew, the crust became thicker. Less dense, more silicic magmas ascended to the surface. A second possible explanation is that changes in the Tharsis plume drove compositional changes of lavas. Baratoux et al. [8] used pMELTS software [44] to model how global magmatism evolved over time from the composition of the primitive martian mantle derived from SNC meteorites [45]. Combined with the thermal evolution of the planet, they showed that the silica concentrations are positively correlated to the degree of partial melting; that is, a higher degree of partial melting generates higher silica concentrations, and vice versa. In addition, the silica concentrations are positively correlated to mantle temperature. The higher temperature of the Tharsis mantle plume [8] generated elevated silica content materials of unit Hsl and Hsu, which erupted after the rise of Tharsis.

6 Conclusions

In this study, we have shown the following.

Firstly, TES spectral analysis shows feldspar, HCP, LCP and high-silica phases are the principal mineral groups for the lava plains in STB. Surface materials of younger units (Hsl and Hsu) have larger amount of high-silica phases (mainly glass) than older units (Hr and HNr).

Secondly, combined with regional stress field and model age of all the geological units, we suggest lava plains in unit HNr and Hr formed before the rise of Tharsis, while lava plains in Hsl and Hsu formed afterward. Compositional variations of the lava plains in STB indicate magma composition may have changed after Tharsis rise. We propose two possible explanations, but the evolution of the magma may be more complex.

Extensive discussions with KRAFT M. and CHRISTENSEN P. are greatly appreciated. The authors thank ROGERS D. for providing the spectral library and DOHM J. for providing the digital version of the geological map. JMARS and Davinci team in ASU, specifically SMITH M. and HAGEE W., supported data processing. MILAM K., PUTZIG N., and FERGASON R. reviewed and improved the manuscript. EDWARDS C., the late GREELEY R., WILLIAMS D., RUFF S. and RYAN A. provided valuable suggestions. This work was supported by China Postdoctoral Science Foundation (Grant No. 2013M540614), the Postdoctoral International Exchange Project, the National Natural Science Foundation of China (Grant No. 41373066), and the Specialized Research Fund for the Doctoral Program of Higher Education (SRFDP) (Grant No. 20130145130001).

1 Werner S C. The global martian volcanic evolutionary history. Icarus, 2009, 201(1): 44–68

2 Xiao L, Huang J, Christensen P R, et al. Ancient volcanism and its implication for thermal evolution of mars. Earth Planet Sc Lett, 2012, 323-324(0): 9–18

3 Carr M H, Head J W. Geologic history of mars. Earth Planet Sc Lett, 2010, 294(3-4): 185–203
4 Carr M H. The Surface of Mars. Cambridge: Cambridge University Press, 2006
5 Beuthe M, Le Maistre S, Rosenblatt P, et al. Density and lithospheric thickness of the tharsis province from MEX MaRS and MRO gravity data. J Geophys Res-Planet, 2012, 117: E04002
6 Baratoux D, Pinet P, Toplis M J, et al. Shape, rheology and emplacement times of small martian shield volcanoes. J Volcanol Geoth Res, 2009, 185(1-2): 47–68
7 Wilson L, Mouginis-Mark P J, Tyson S, et al. Fissure eruptions in tharsis, mars: Implications for eruption conditions and magma sources. J Volcanol Geoth Res, 2009, 185(1-2): 28–46
8 Baratoux D, Toplis M J, Monnereau M, et al. Thermal history of mars inferred from orbital geochemistry of volcanic provinces. Nature, 2011, 472(7343): 338–341
9 Bandfield J L. Global mineral distributions on Mars. J Geophys Res-Planet, 2002, 107(E6): 9
10 Poulet F, Gomez C, Bibring J P, et al. Martian surface mineralogy from Observatoire pour la Minéralogie, l'Eau, les Glaces et l'Activité on board the Mars Express spacecraft (OMEGA/MEx): Global mineral maps. J Geophys Res-Planet, 2007, 112(E8), doi:10.1029/2006JE002840
11 Rogers A D, Christensen P R. Surface mineralogy of martian low-albedo regions from MGS-TES data: Implications for upper crustal evolution and surface alteration. J Geophys Res-Planet, 2007, 112(E1), doi: 10.1029/2006JE002727
12 Ody A, Poulet F, Langevin Y, et al. Global maps of anhydrous minerals at the surface of mars from OMEGA/MEx. J Geophys Res-Planet, 2012, 117, doi: 10.1029/2012je004117
13 Ruff S W, Christensen P R. Bright and dark regions on mars: Particle size and mineralogical characteristics based on thermal emission spectrometer data. J Geophys Res-Planet, 2002, 107(E12): 2
14 Lang N P, Tornabene L L, McSween H Y, et al. Tharsis-sourced relatively dust-free lavas and their possible relationship to martian meteorites. J Volcanol Geoth Res, 2009, 185(1-2): 103–115
15 Dohm J M, Tanaka K L. Geology of the thaumasia region, mars: Plateau development, valley origins, and magmatic evolution. Planet Space Sci, 1999, 47(3-4): 411–431
16 Tanaka K L, Davis P A. Tectonic history of the syria planum province of mars. J Geophys Res-Solid, 1988, 93(B12): 14893–14917
17 Anderson R C, Dohm J M, Golombek M P, et al. Primary centers and secondary concentrations of tectonic activity through time in the western hemisphere of Mars. J Geophys Res-Planet, 2001, 106(E9): 20563–20585
18 Baptista A R, Mangold N, Ansan V, et al. A swarm of small shield volcanoes on syria planum, Mars. J Geophys Res-Planet, 2008, 113(E9), doi:10.1029/2007JE002945
19 Plescia J B, Golombek M P. Origin of planetary wrinkle ridges based on the study of terrestrial analogs. Geol Soc Am Bull, 1986, 97(11): 1289–1299
20 Schultz RA. Localization of bedding plane slip and backthrust faults above blind thrust faults: Keys to wrinkle ridge structure. J Geophys Res-Planet, 2000, 105(E5): 12035–12052
21 Golombek M P, Anderson F S, Zuber M T. Martian wrinkle ridge topography: Evidence for subsurface faults from mola. J Geophys Res-Planet, 2001, 106(E10): 23811–23821
22 Dohm J M, Tanaka K L, Hare T M. Geological map of the thaumasia region, Mars. U.S. Geological Survey Geologic Investigations Series I-2650, 2001 (Available at http://pubs.usgs.gov/imap/i2650/)
23 Putzig N E, Mellon M T. Apparent thermal inertia and the surface heterogeneity of Mars. Icarus, 2007, 191(1): 68–94
24 Christensen P R, Bandfield J L, Hamilton V E, et al. Mars Global Surveyor Thermal Emission Spectrometer experiment: Investigation description and surface science results. J Geophys Res-Planet, 2001, 106(E10): 23823–23871
25 Presley M A, Christensen P R. Thermal conductivity measurements of particulate materials. 2. Results. J Geophys Res-Planet, 1997, 102(E3): 6551–6566
26 Fergason R L, Christensen P R, Kieffer H H. High-resolution thermal inertia derived from the thermal emission imaging system (THEMIS): Thermal model and applications. J Geophys Res-Planet, 2006, 111(E12), doi: 10.1029/2006JE002735
27 Mellon M T, Jakosky B M, Kieffer H H, et al. High-resolution thermal inertia mapping from the Mars global surveyor thermal emission spectrometer. Icarus, 2000, 148(2): 437–455
28 Williams D A, Greeley R, Manfredi L, et al. Surface-compositional properties of the Malea Planum region of the Circum-Hellas Volcanic Province, Mars. Earth Planet Sc Lett, 2010, 294(3-4): 451–465
29 Rogers A D, Bandfield J L, Christensen P R. Global spectral classification of martian low-albedo regions with mars global surveyor thermal emission spectrometer (MGS-TES) data. J Geophys Res-Planet, 2007, 112(E2), doi: 10.1029/2006JE002726
30 Bandfield J L, Hamilton V E, Christensen P R. A global view of martian surface compositions from MGS-TES. Science, 2000, 287(5458): 1626–1630
31 Smith M D, Bandfield J L, Christensen P R. Separation of atmospheric and surface spectral features in mars global surveyor thermal emission spectrometer (TES) spectra. J Geophys Res-Planet, 2000, 105(E4): 9589–9607
32 Ramsey M S, Christensen P R. Mineral abundance determination: Quantitative deconvolution of thermal emission spectra. J Geophys Res-Sol Ea, 1998, 103(B1): 577–596
33 Rogers A D, Aharonson O. Mineralogical composition of sands in meridiani planum determined from mars exploration rover data and comparison to orbital measurements. J Geophys Res-Planet, 2008, 113(E6), doi: 10.1029/2007JE002995
34 Christensen P R, Bandfield J L, Smith M D, et al. Identification of a basaltic component on the martian surface from thermal emission spectrometer data. J Geophys Res-Planet, 2000, 105(E4): 9609–9621
35 Huang J, Edwards C S, Horgan B H N, et al. Identification and mapping of dikes with relatively primitive compositions in thaumasia planum on Mars: Implications for tharsis volcanism and the opening of valles marineris. Geophys Res Lett, 2012, 39(17), doi: 10.1029/2012gl052523
36 Wilson L, Head J W. Tharsis-radial graben systems as the surface manifestation of plume-related dike intrusion complexes: Models and implications. J Geophys Res-Planet, 2002, 107(E8), doi: 10.1029/2001je001593
37 Andrews-Hanna J C. The formation of valles marineris: 2. Stress focusing along the buried dichotomy boundary. J Geophys Res-Planet, 2012, 117(E4), doi: 10.1029/2011je003954
38 Greeley R, Leach R N, Williams S H, et al. Rate of wind abrasion on Mars. J Geophys Res-Planet, 1982, 87(Nb12): 9–24
39 Sagan C, Veverka J, Fox P, et al. Variable features on Mars, 2, Mariner-9 global results. J Geophys Res-Planet, 1973, 78(20): 4163–4196
40 Hartmann W K, Neukum G. Cratering chronology and the evolution of Mars. Space Sci Rev, 2001, 96(1-4): 165–194
41 Boynton W V, Taylor G J, Evans L G, et al. Concentration of h, si, cl, k, fe, and th in the low- and mid-latitude regions of Mars. J Geophys Res-Planet, 2007, 112(E12), doi: 10.1029/2007JE002887
42 Hauber E, Bleacher J, Gwinner K, et al. The topography and morphology of low shields and associated landforms of plains volcanism in the Tharsis region of Mars. J Volcanol Geoth Res, 2009, 185(1-2): 69–95
43 Huang J, Xiao L, Kraft M D, et al. Surface-compositional properties of lava plains in syria-thaumasia block, Mars. 2012 AGU Fall Meeting abstract, id: P11E–1857
44 Ghiorso M S, Hirschmann M M, Reiners P W, et al. The pmelts: A revision of melts for improved calculation of phase relations and major element partitioning related to partial melting of the mantle to 3 gpa. Geochem Geophy Geosy, 2002, 3: 1–35
45 Dreibus G, Wanke H. Mars, a volatile-rich planet. Meteoritics, 1985, 20(2): 367–381
46 Christensen P R, Bandfield J L, Hamilton V E, et al. A thermal emission spectral library of rock-forming minerals. J Geophys Res-Planet, 2000, 105(E4): 9735–9739
47 Smith D E, Zuber M T, Frey H V, et al. Mars orbiter laser altimeter: Experiment summary after the first year of global mapping of mars. J Geophys Res-Planet, 2001, 106(E10): 23689–23722